PROCEEDINGS OF SCIENCE

Correlations of the multiwavelength emission in the blazar CTA 102 during 2016–2018

Sang-Hyun Kim[a,b,*] **and Sang-Sung Lee**[a,b]

[a] *Korea Astronomy and Space Science Institute, 776 Daedeok-daero, Yuseong-gu, Daejeon 34055, Korea*

[b] *Astronomy and Space Science, University of Science and Technology, 217 Gajeong-ro, Yuseong-gu, Daejeon 34113, Korea*

E-mail: sanghkim@kasi.re.kr, sslee@kasi.re.kr

Blazars are among the most powerful objects in the universe. Their relativistic jets pointing towards Earth show variable flux density across the entire electromagnetic spectrum. The Fermi Large Area Telescope observed the active γ-ray states in the blazar CTA 102 from 2016 to 2018. During this period, we found two prominent γ-ray flares. In this study, we investigated correlations of the multiwavelength emission to figure out the nature of the γ-ray flares by employing the discrete correlation function. The γ-ray flare in 2016 December showed 3σ correlations with optical and X-ray flares, while radio counterparts are not clearly shown. We found that the γ-ray flare in 2018 January is correlated with radio and optical flares above 2σ confidence levels, yielding time lags of less than 30 days. We used the 43 GHz Very Long Baseline Array (VLBA) data to explore the kinematics and flux variability in the parsec-scale jet of this source during the γ-ray flares. The 2018 γ-ray flare is associated with an ejection of a new jet component from the radio core. We found that the γ-ray (F_γ) and optical (F_O) fluxes are significantly correlated as $F_\gamma \propto F_\mathrm{O}^m$ ($m = 0.60 - 1.17$), suggesting that the external Compton scattering is the dominant emission mechanism for the two γ-ray flares.

15th European VLBI Network Mini-Symposium and Users' Meeting (EVN2022)
11-15 July 2022
University College Cork, Ireland

*Speaker

PoS(EVN2022)013

1. Introduction

Radio-loud active galactic nuclei (AGNs) launch relativistic jets which are luminous and collimated outflows. According to unified schemes, the radio-loud AGNs are classified as blazars when their jets are closely aligned with our line of sight [44], yielding most likely rapid variability, relativistically boosted emission, and superluminal jet motions [7, 14]. Very long baseline interferometry (VLBI) observations of blazars with milliarcsecond(mas)-scale resolutions show superluminal jet components. A compact bright region at the upper end of the jet is referred to as the core and other ones downstream of the jet are called jet components (e.g., [27]).

The γ-ray observations with the Large Area Telescope (LAT) on board the Fermi γ-ray space telescope have revealed that blazars constitute the most significant fraction of the γ-ray sources in the extragalactic sky (e.g., [1–3, 6, 33]). The γ-ray flares in blazars generally display extreme flux enhancements in time. However, the origin of γ-ray flares is still under debate, depending on sources and flares. The γ-ray emission from relativistic jets is commonly attributed to the inverse-Compton (IC) scattering of low-energy photons off relativistic electrons from synchrotron radiation in jets of the sources [20, 30]. The seed photons which are responsible for the IC scattering come from the jet itself or external to the jet (e.g., the broad-line region (BLR), the narrow-line region (NLR), the dusty torus, and the cosmic microwave background radiation). For the former case, the IC scattering is referred to as synchrotron self-Compton (SSC, e.g., [31]) and for the latter one, it is called external IC (EC, e.g., [13]). The γ-ray flares are often accompanied by flares at other wavelengths (e.g., radio, optical, and X-ray, etc.). Significant correlations between γ-ray and radio flares have been reported, suggesting that γ-ray flares are most likely to occur in the parsec-scale jets [4, 23, 32]. A remarkable correlation between γ-ray and optical flares gives us a hint of the physical mechanism of γ-ray flares, for example, SSC or EC [26, 29]. Therefore, the correlation study using multiwavelength light curves is crucial to understand the nature of γ-ray flares in blazar jets.

CTA 102 ($z = 1.037$) is one of the γ-ray bright blazars and shows variability at radio to γ-rays (e.g., [8, 12]). The multiwavelength radio variability of the source was investigated from 2012 to 2018, including month-scale variability at 15 GHz [24]. The Fermi-LAT detected γ-ray activity from CTA 102. The source reached its highest γ-ray flux in 2016 December, which was recorded as one of the brightest γ-ray flares in blazars [10]. The other strong γ-ray flare was observed from 2017 to 2018 [19]. Studies on the γ-ray flare in 2016–2017 have been reported (e.g., [9, 12, 18, 22, 38, 40, 49]). However, few studies explored the γ-ray flare in 2017–2018 [19, 41]. They did not examine a correlation of this γ-ray flare with radio ones.

We aim to figure out the location and physical mechanism of γ-ray flares in CTA 102 during the period from 2016 to 2018, providing the first results of examining a correlation between γ-ray and radio flares during 2017–2018. We present results from this work, including multiwavelength correlations with respect to the γ-ray light curve and kinematics of the radio jet related to γ-ray flares. Throughout this study, we adopt a flat ΛCDM cosmology with $\Omega_{\rm m} = 0.315$, $\Omega_\Lambda = 0.685$, and $H_0 = 67.4\,{\rm km\ s^{-1}\ Mpc^{-1}}$ [37]. The luminosity distance at a redshift of the source (i.e., $z = 1.037$) is $D_{\rm L} = 7112.9$ Mpc and a linear scale is 8.311 pc mas^{-1}, calculated with the Cosmology Calculator[1] [48]. A proper motion of 1 mas yr^{-1} corresponds to 55.2 c.

[1] https://astro.ucla.edu/~wright/CosmoCalc.html

2. Observations and Data

We made use of the radio data which covers a period from 2012 November to 2018 September (MJD 56251–58384), with a frequency range of 15–343 GHz. The data are complemented by the Owens Valley Radio Observatory (OVRO) 40-m radio telescope at 15 GHz, the Metsähovi 13.7-m radio telescope at 37 GHz, the IRAM 30-m Telescope at 86 and 230 GHz, the SMA at 230 and 340 GHz, the Atacama Large millimeter/submillimeter Array (ALMA) at 91, 233, and 343 GHz, and the Very Long Baseline Array (VLBA) at 43 GHz (for more details and references for the data, see [24]). We used the optical data available from the optical spectropolarimetric monitoring program at Steward Observatory of the University of Arizona in optical V-and R-bands[2] [43]. The data spans a period from 2012 October to 2018 July (MJD 56211–58306). We collected the X-ray data at 14–195 keV from the Neil Gehrels Swift Observatory/Burst Alert Telescope (*Swift*/BAT) 157-Month Hard X-ray Survey[3]. The data spans a period from 2012 September 29 to 2017 December 30 (MJD 56200–58118). We made use of the γ-ray data at photon energies of 0.1–300 GeV from the Fermi-LAT, spanning from 2012 September 29 to 2018 October 8 (MJD 56200–58400) (e.g., [2]).

3. Results

3.1 Multi-wavelength light curves

Multiwavelength light curves from CTA 102 at radio, optical, X-rays, and γ-rays cover a time range from 2012 September to 2018 October (MJD 56200–58394). The source is relatively stable in brightness at γ-rays with photon flux densities of $F_\gamma \leq 2\times10^{-6}$ ph cm^{-2} s^{-1} until late 2015. The source displays multiple γ-ray activities after 2016. In order to define a γ-ray flare, we regarded a threshold as the mean plus the standard deviation of the flux density [e.g., 5, 24]. Considering this threshold (2.7×10^{-6} ph cm^{-2} s^{-1}), we found six flares (Flare 1–6) in the γ-ray light curve. Flare 3 is found to be the strongest γ-ray flare with a peak of $(1.415 \pm 0.018) \times 10^{-5}$ ph cm^{-2} s^{-1} on 2016 December 27 (MJD 57750).

We visually inspected the source and found that the γ-ray flares seem to be associated with the flares at the other energies. Considering the sufficient number of data points, we focused on Flare 3 and Flare 6. Table 1 summarizes multiwavelength flares seen in a period of Flare 3 or Flare 6. We found that optical and X-ray flares are close in time to Flare 3, implying a short time lag between Flare 3 and X-ray and optical flares. We note that Flare 6 is likely to be correlated with multiple flares at radio and optical wavelengths.

We investigated the statistical properties of multi-wavelength light curves, the power spectral density (PSD), and the probability density function (PDF). We followed [5] for the analysis of the PSD and PDF. In order to compute them, we used the public code by [11], based on the model implementation described in [16]. The PSD model represents the variability power as a function of temporal frequency [46]. We used a power-law spectrum for fitting the PSD [45]. The PDFs for the flux density of the source in the light curves display a gamma distribution for the optical and γ-ray light curves and a log-normal distribution for the radio and X-ray light curves. We found that PSD

[2] http://james.as.arizona.edu/~psmith/Fermi/
[3] https://swift.gsfc.nasa.gov/results/bs157mon/1155

Table 1: Multiwavelength flares near Flares 3 and 6

ID	Frequency Band	Peak time		Peak Flux density
		Date	MJD	
(1)	(2)	(3)	(4)	(5)
Flare 3	R-band	2016-12-30	57752	116 ± 7 mJy
	V-band	2016-12-30	57752	88 ± 4 mJy
	X-ray	2017-01-30	57783	$(5.231 \pm 0.744) \times 10^{-3}$ count/s
Flare 6	15 GHz	2018-02-16	58165	3.99 ± 0.04 Jy
	37 GHz	2018-01-18	58158	6.30 ± 0.27 Jy
	89 GHz	2018-01-12	58130	10.52 ± 0.53 Jy
	230 GHz	2018-01-12	58130	8.94 ± 0.45 Jy
	R-band	2017-12-16	58104	15.24 ± 0.98 mJy
	V-band	2017-12-16	58104	10.58 ± 0.29 mJy

Note. Column designation: (1) name of a γ-ray flare, (2) Frequency band whose flare is seen during a γ-ray flare, (3) peak time of a flare in year-month-day (4) peak time of a flare in modified Julian date (MJD), and (5) flux density of a flare at a frequency band.

slopes at all wavelengths are $\geq \sim 1$, corresponding to red noise that the power spectra of AGN light curves generally show (e.g., [34].

3.2 Correlation analysis

In order to study the correlation and time lags for an unevenly sampled data set, we used the discrete correlation function (DCF) [15]. A positive (negative) time lag indicates that the flux density at a higher frequency leads (lags) the flux density at a lower frequency. To calculate this, we used the public code of the DCF to be implemented in Python by [39]. For a frequency pair, we considered the lag bin width ($\Delta t_{\rm bin}$) as the mean cadence ($t_{\rm int}$) of the less frequently sampled light curve. An optimal bin width was found in a range of $t_{\rm int} - 2t_{\rm int}$. We selected a time lag range whose length covers at least a 2/3 fraction of the light curves (e.g., [28]).

We simulated 10,000 artificial light curves with statistical properties (i.e., the PSD and PDF) similar to real ones for each frequency pair to investigate the significance of the DCF. We then calculated the DCFs of the simulated light curves and obtained 10,000 DCFs used to estimate 1σ, 2σ, and 3σ (68%, 95%, and 99.7%, respectively) confidence levels. We considered that the DCFs above 2σ (95%) are statistically significant. To measure the uncertainties of DCF peaks ($\rm DCF_{peak}$) and corresponding time lags ($\tau_{\rm DCF}$), we used the flux randomization and random subset selection (FRRSS) method [35]. We simulated 10,000 artificial light curves randomly sampled from a light curve. Then, we performed the DCF analysis to obtain 10,000 $\rm DCF_{peak}$ and $\tau_{\rm DCF}$ for a frequency pair. Based on them, the distributions for $\rm DCF_{peak}$ and $\tau_{\rm DCF}$ can be obtained. We fitted a Gaussian function to each DCF (i.e., $\rm DCF_{peak}$ and $\tau_{\rm DCF}$) distribution. The mean and standard deviation of the fitted Gaussian are considered to be the fitted value and uncertainty for $\rm DCF_{peak}$ and $\tau_{\rm DCF}$, respectively.

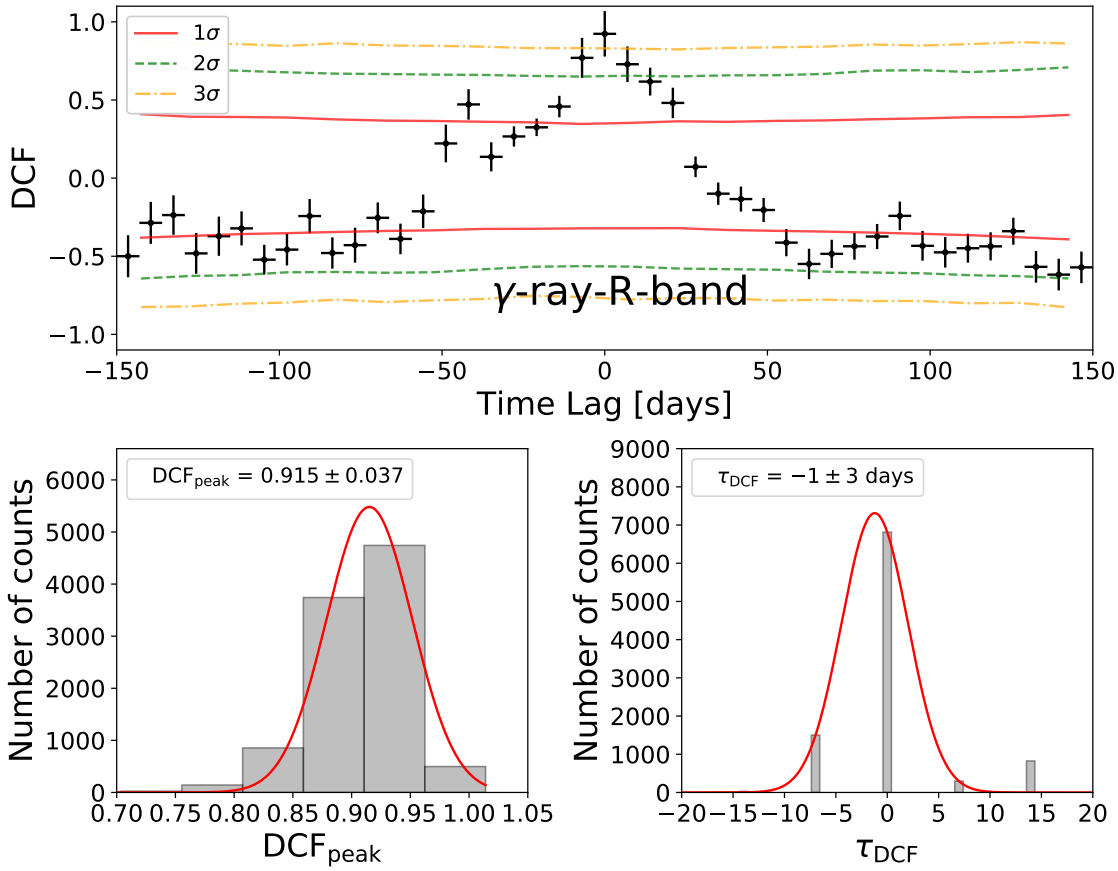

Figure 1: Top: DCF for γ-ray versus R-band. The red solid, green dashed, and orange dot-dashed lines indicate 1σ, 2σ, and 3σ, respectively (see the label). Bottom: Distributions for $\mathrm{DCF_{peak}}$ (left) and τ_{DCF} (right). The red solid line corresponds to a Gaussian fit to each distribution. See the label for the best-fit values and uncertainties of the fit parameters.

To explore multiwavelength correlations with regard to Flare 3, we performed the DCF analysis during the period of 2016 July 30–2017 May 26 (MJD 57600–57900). We found that optical (i.e., R-and V-bands) and X-ray flares are tightly correlated with Flare 3 above 3 σ, yielding nearly zero time lags within their uncertainties. This implies that optical, X-ray, and γ-ray flares are co-spatial. Figure 1 displays a DCF result of R-band–γ-ray pair during the period of Flare 3. Contrary to the evident correlation among flares at the other bands, the correlation between radio flares and Flare 3 is complicated. While radio fluxes enhanced near the time of Flare 3, a radio counterpart to Flare 3 is not clearly shown. Our result is consistent with [12].

We conducted the DCF analysis to find multiwavelength flares correlated with Flare 6 during the period from 2017 September 3 to 2018 October 8 (MJD 58000–58400), except for 343 GHz and X-rays due to the lack of data. For the 89 GHz–γ-ray pair, we could not estimate τ_{DCF} and its uncertainty as this shows a bimodal distribution. Figure 2 displays τ_{DCF} of CTA 102 during Flare 6. Time lags were all estimated to be < 30 days. We note positive time lags between the γ-ray and radio light curves, implying that the γ-ray emission region is located upstream of the radio emission

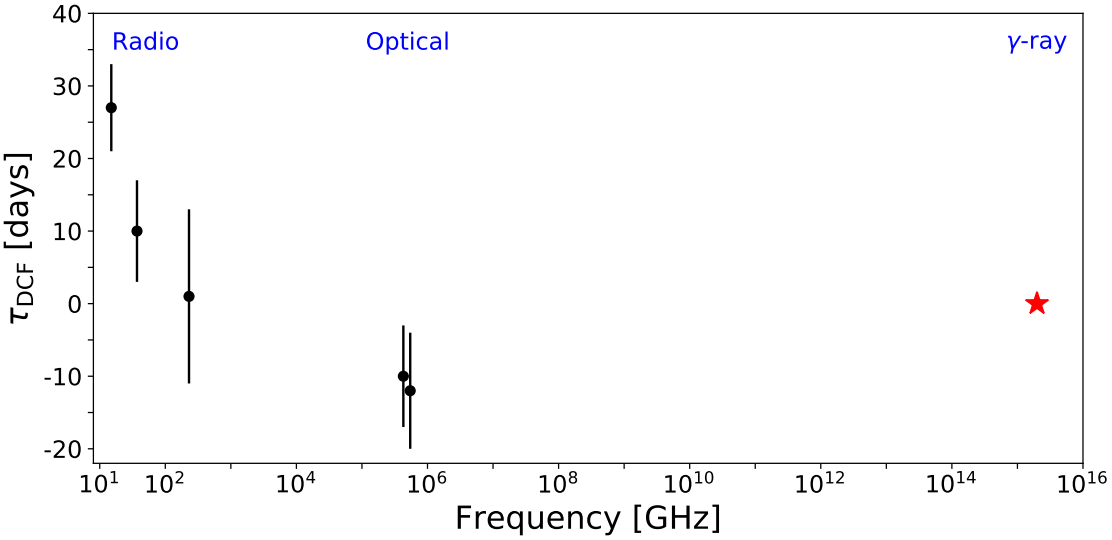

Figure 2: Time lag ($\tau_{\rm DCF}$) between γ-ray and other bands. The red star denotes the γ-ray as a reference frequency.

region.

3.3 Jet kinematics

To parameterize the compact bright features in the source, we performed the model-fitting analysis of the VLBA data using the *MODELFIT* task in the interferometric imaging software `DIFMAP` [42]. Multiple components for each epoch were obtained by fitting circular two-dimensional Gaussian models to the CLEAN images. The jet parameters are flux densities, relative distances from the core (R), sizes, and relative position angles with respect to the core (PA), which were estimated with their uncertainties following [21, 47]. We designated the core as C0 and the jet components as C ($<$ ~0.2 mas separated from the core) or J (nearly stationary) with a number depending on the distance from the core. Following the formalism in [21, 47], we derived the physical parameters of the moving jet components, for example, the apparent speed ($\beta_{\rm app}$), the variability Doppler factor ($\delta_{\rm var}$), the Lorentz factor (Γ), and the viewing angle ($\theta_{\rm obs}$), etc. The ejection time of a jet component is defined as the time when the centroid of the jet component coincides with the centroid of the core.

Figure 3 displays the separation of jet components from the core as a function of time. For the data period, two jet components of C2 and C3 were ejected from the core and moved downstream of the jet. The ejection time of C2 is 2016 June 5 (MJD57545^{+24}_{-23}), which is apart from Flare 3. This implies that the interaction between C0 and C2 is not likely to be related to this flare. We found that C2 passed through C1 when Flare 3 reached a peak. The variability Doppler factor of C2 is $\delta_{\rm var} = 12.192^{+2.243}_{-2.079}$. Considering the lower limit for the Doppler factor at the γ-rays ($\geq$ 15) [9], our estimation of $\delta_{\rm var}$ cannot satisfy to explain Flare 3. Therefore, we conclude that C2 seems to be not associated with Flare 3.

We investigated the connection of C3 with Flare 6. The variability Doppler factor of C3 is

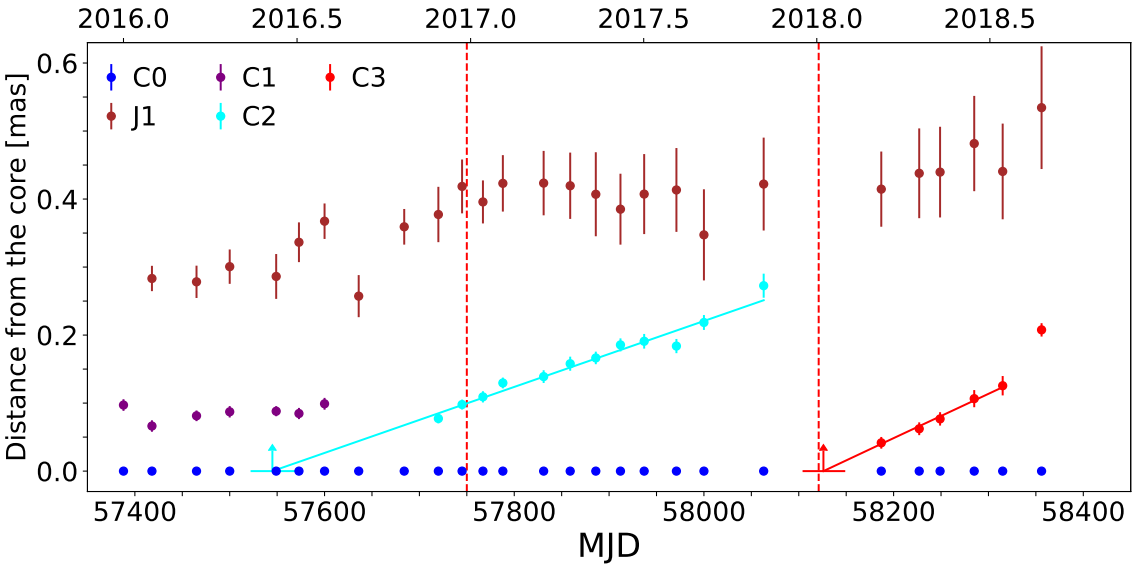

Figure 3: Separation of jet components from the core. The red vertical dashed lines indicate a peak of Flares 3 and 6. Upward arrows and horizontal lines correspond to the ejection times of jet components and their uncertainties.

$\delta_{\rm var} = 37.775^{+5.937}_{-6.295}$, which is compatible with the estimate of $\delta_{\rm var}$ in [47]. Figure 4 presents the VLBA 43 GHz images of CTA 102 after Flare 6. The ejection time of C3 is 2018 January 7 corresponding to MJD58126$^{+23}_{-22}$. In the 7-day bin γ-ray light curve, Flare 6 peaked on 2018 January 2 (MJD 58121), which is consistent with the ejection of C3. The 1-day bin γ-ray light curve also confirmed the time coincidence between Flare 6 and the emergence of C3 from C0. Therefore, we suggest that the interaction between C3 and C0 is associated with Flare 6.

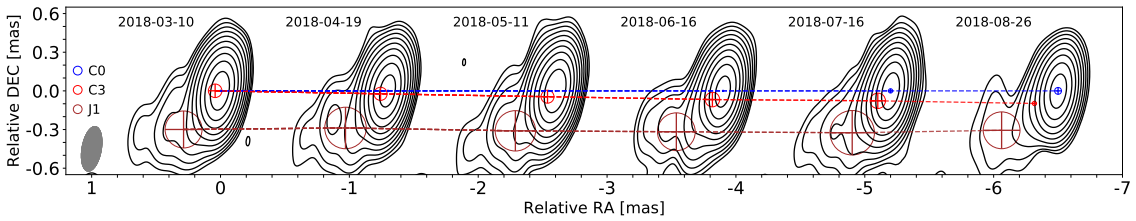

Figure 4: 43 GHz VLBA maps of CTA 102 with fitted Gaussian components. The epoch of the observations is presented above each contour map. The contours increase by a factor of two from the lowest level. The lowest levels are 3.22, 3.11, 1.87, 2.32, 3.04, and 4.11 mJy beam^{-1} from left to right. All maps are restored with a common beam of 0.35×0.15 mas at -10 deg (illustrated at the bottom left-hand panel). The circles with crosses show the position and size of the Gaussian components. The dashed lines indicate the evolution of jet components.

4. Discussion

We found significant correlations between the γ-ray and optical emissions in Flares 3 and 6. To understand the emission mechanisms of these flares, we examined the γ-ray and optical

flux correlations. We assume that synchrotron radiation from the jet is mostly emitted at optical wavelength, whereas the γ-ray emission is from IC scattering of optical/IR photons by relativistic electrons in the jet (e.g., [26, 29]). Under the assumption, the relation of the flux density of the IC scattered emission ($F_{\rm IC}$) and that of the synchrotron radiation ($F_{\rm sync}$) is the following: $F_{\rm IC} \propto F_{\rm sync}^{m}$, where m is a slope of the flux–flux relation. If the EC scattering dominates the emission mechanism, the slope would be $m = 1$. While if the SSC is the dominant emission mechanism, the slope would be $m = 2$. We performed the Pearson correlation analysis and computed Pearson correlation coefficients ($r_{\rm p}$) and p-values ($p_{\rm value}$) to explore the degrees of correlation between the γ-ray and optical emissions. We then fitted a linear function to the γ-ray–optical flux densities on a logarithmic scale. For both Flares 3 and 6, the Pearson correlations coefficients are $r_{\rm p} > 0.8$ with significance levels ($1 - p_{\rm value}$) above 99.99%. In addition, the slopes of the flux–flux relation are close to unity during both Flares 3 and 6, suggesting that the EC scattering is the dominant emission mechanism for those flares.

We discuss the candidates of seed photons that contribute to γ-ray flares. The BLR radius in CTA 102 is 6.73×10^{17} cm [36]. The size of the torus is 6.43×10^{18} cm [18]. Combining time lags and physical parameters of C3, we constrained the location of the γ-ray emission region as a 5–14 pc ($\sim 10^{19}$ cm) from the jet base during the period of Flare 6 (for the analysis, see [25]). We note that the location of the γ-ray emission region is closer to the torus than the BLR. Moreover, a model of the seed photons radiation fields presents that the seed photons from the torus mostly result in the γ-ray emission when the γ-ray emission region is located at 10^{19} cm from the central engine [17]. Therefore, photons from the torus can be a candidate for the seed photons to generate Flare 6. We could not constrain the location of the γ-ray emission region during the period of Flare 3. The cross-correlation result presented that Flare 3 is co-spatial with the optical and X-ray flares, whereas this flare has no radio counterpart, implying that the γ-ray emission region might be located further upstream of the radio core. As studies suggested (e.g., [18, 41]), both the BLR and torus photons can be a candidate for seed photons that contributes to Flare 3.

5. Conclusions

The blazar CTA 102 showed γ-ray flaring activity from 2016 to 2018. We found two prominent γ-ray flares peaking in 2016 December and 2018 January, respectively. We studied the physical origin of γ-ray flares in CTA 102 by investigating the cross-correlation between γ-ray flares and flares at other bands. The cross-correlation results present that the 2016 γ-ray flare is co-spatial with optical and X-ray flares. However, this γ-ray flare has no radio counterparts, implying that the γ-ray emission region is upstream of the radio one. The 2018 γ-ray flare showed significant correlations with radio and optical flares. A new jet component was ejected during the 2018 γ-ray flare, which indicates that the interaction between the core and the jet component is associated with this flare. During both γ-ray flares in 2016 and 2018, the relation between the γ-ray and optical fluxes is linear, which is consistent with the EC mechanism. We speculate that the γ-ray flare in 2016 December might be explained if the BLR and/or torus photons are the seed photons in the EC process. The location of the γ-ray emission region in 2018 was constrained to be 5–14 pc from the jet base. The close distance between the γ-ray emission region and the torus suggests that the torus photons contribute to the 2018 γ-ray flare.

References

[1] Abdo, A. A., Ackermann, M., Ajello, M., et al., 2010, ApJS, 188, 405

[2] Abdollahi, S., Acero, F., Ackermann, M., et al., 2020, ApJS, 247, 33

[3] Acero, F., Ackermann, M., Ajello, M., et al., 2015, ApJS, 218, 23

[4] Agudo, I., Jorstad, S. G., Marscher, A. P., et al., 2011, ApJL, 726, L13

[5] Algaba, J.-C., Lee, S.-S., Kim, D.-W., et al., 2018, ApJ, 852, 30

[6] Atwood, W. B., Abdo, A. A., Ackermann, M., et al., 2009, ApJ, 697, 1071

[7] Blandford, R. D., McKee, C. F., Rees, M., J., 1977, Nature, 267, 211

[8] Casadio, C., Gómez, J. L., Jorstad, S. G., et al., 2015, ApJ, 813, 51

[9] Casadio, C., Marscher, A. P., Jorstad, S. G., et al., 2019, A&A, 622, A158

[10] Ciprini, S., 2016, ATel, 9869, 1

[11] Connolly, S. D., 2015, arXiv e-prints, arXiv:1503.06676

[12] D'Ammando, F., Raiteri, C. M., Villata, M., et al., 2019, MNRAS, 490, 5300

[13] Dermer, C. D., Schlickeiser, R., Mastichiadis, A., 1992, A&A, 256, L27

[14] Dondi, L., Ghisellini, G., 1995, MNRAS, 273, 583

[15] Edelson, R. A., Krolik, J. H., 1988, ApJ, 333, 646

[16] Emmanoulopoulos, D., McHardy, I. M., Papadakis, I. E., 2013, MNRAS, 433, 907

[17] Finke, J. D., 2016, ApJ, 830, 94

[18] Gasparyan, S., Sahakyan, N., Baghmanyan, V., et al., 2018, ApJ, 863, 114

[19] Geng, X., Ding, N., Cao, G., et al., 2022, ApJS, 260, 48

[20] Hovatta, T., Lindfors, E., 2019, NewAR, 87, 101541

[21] Jorstad, S. G., Marscher, A. P., Morozova, D. A., et al., 2017, ApJ, 846, 98

[22] Kaur, N., Baliyan, K. S., 2018, A&A, 617, A59

[23] Kim, D.-W., Kravchenko, E. V., Kutkin, A. M., et al., 2022, ApJ, 925, 64

[24] Kim, S.-H., Lee, S.-S., Lee, J., W., et al., 2022, MNRAS, 510, 815

[25] Kudryavtseva, N. A., Gabuzda, D. C., Aller, M. F., et al., 2011, MNRAS, 415, 1631

[26] Larionov, V. M., Villata, M., Raiteri, C. M., et al., 2016, MNRAS, 461, 3047

[27] Lee, S.-S., Wajima, K., Algaba, J.-C., et al., 2016, ApJS, 227, 8

[28] Liodakis, I., Romani, R. W., Filippenko, A. V., et al. 2018, MNRAS, 480, 5517

[29] Liodakis, I., Romani, R. W., Filippenko, A. V., et al., 2019, ApJ, 880, 32

[30] Madejski, G. G., Sikora, M., 2016, ARA&A, 54, 725

[31] Maraschi, L., Ghisellini, G., Celotti, A., 1992, ApJL, 397, L5

[32] Max-Moerbeck, W., Hovatta, T., Richards, J. L., et al., 2014, MNRAS, 445, 428

[33] Nolan, P. L., Abdo, A. A., Ackermann, M., et al., 2012, ApJS, 199, 31

[34] Park, J.-H., Trippe, S., 2014, ApJ, 785, 76

[35] Peterson, B. M., Wanders, I., Horne, K., et al., 1998, PASP, 110, 660

[36] Pian, E., Falomo, R., Treves, A., 2005, MNRAS, 361, 919

[37] Planck Collaboration, Aghanim, N., Akrami, Y., et al., 2020, A&A, 641, A6

[38] Prince, R., Raman, G., Hahn, J., et al., 2018, ApJ, 866, 16

[39] Robertson, D. R. S., Gallo, L. C., Zoghbi, A., et al., 2015, MNRAS, 453, 3455

[40] Sahakyan, N., 2020, A&A, 635, A25

[41] Sahakyan, N., Israyelyan, E., Harutyunyan, G., et al., 2022, MNRAS, 5157, 2757

[42] Shepherd, M. C. 1997, in Astronomical Society of the Pacific Conference Series, Vol. 125, Astronomical Data Analysis Software and Systems VI, ed. G. Hunt & H. Payne, 77

[43] Smith, P. S., Montiel, E., Rightley, S., et al., 2009, arXiv:0912.3621

[44] Urry, C. M., Padovani, P., 1995, PASP, 107, 803

[45] Uttley, P., McHardy, I. M., Papadakis, I. E., 2002, MNRAS, 332, 231

[46] Vaughan, S., Edelson, R., Warwick, R. S., 2003, MNRAS, 345, 1271

[47] Weaver, Z. R., Jorstad, S. G., Marscher, A. P., et al., 2022, ApJS, 260, 12

[48] Wright, E. L., 2006, PASP, 118, 1711

[49] Zacharias, M., Böttcher, M., Jankowsky, F., et al., 2017, ApJ, 851, 72